Submitted to
Physical Review D

LBL-3306
Preprint

THE REACTIONS $K^- p \to \Sigma^0 \pi^0$ AND $K^- p \to \Lambda \pi^0$ IN THE MOMENTUM RANGE 240 TO 450 MeV/c

T. S. Mast, M. Alston-Garnjost, R. O. Bangerter,
A. S. Barbaro-Galtieri, F. T. Solmitz and R. D. Tripp

August 1974

Prepared for the U. S. Atomic Energy Commission
under Contract W-7405-ENG-48

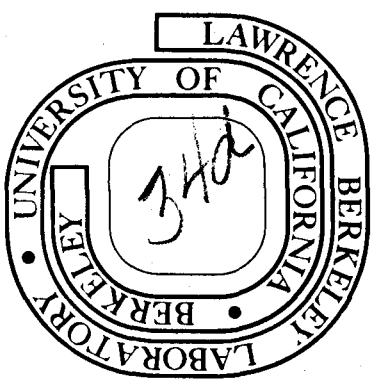

LBL-3306

DISCLAIMER

LBL-3306

THE REACTIONS $K^-p \to \Sigma^0\pi^0$ AND $K^-p \to \Lambda\pi^0$ IN THE MOMENTUM RANGE 240 to 450 MeV/c *

T. S. Mast, M. Alston-Garnjost, R. O. Bangerter,
A. S. Barbaro-Galtieri, F. T. Solmitz and R. D. Tripp

Lawrence Berkeley Laboratory
University of California
Berkeley, California 94720

ABSTRACT

An analysis has been made of 57,600 events of the type $K^-p \to \Lambda$ + missing neutrals obtained in the Berkeley 25-inch hydrogen bubble chamber. The data were divided into intervals of 10 MeV/c in incident momentum and fits were made to the distribution in missing neutral mass, the production cosine, and the polarization of the lambda. These fits yielded Legendre coefficients describing the cross sections and polarizations for $K^-p \to \Sigma^0\pi^0$ and $K^-p \to \Lambda\pi^0$ in the momentum range 240 to 450 MeV/c. The cross sections and polarization in the $\Sigma^0\pi^0$ final state show marked structure coming from the production and decay of Λ (1520). The cross sections and polarizations for the $\Lambda\pi^0$ final state vary slowly. No new structure is observed.

I. INTRODUCTION

In the region near 400 MeV/c incident momentum the major structure in the K^-p channel is the $\Lambda(1520)$.[1] As part of a detailed study of all the final states in this region[2] we report here on the $\Sigma^0\pi^0$ and $\Lambda\pi^0$ final states. Data on the $\Sigma^0\pi^0$ final state coupled with that for $\Sigma^{\pm}\pi^{\mp}$ provide a test of charge independence[3] and a strong constraint on partial wave analyses in this region. The $\Lambda\pi^0$ final state is pure I = 1 and the $\Sigma^0\pi^0$ final state is pure I = 0.

A sample of 57,600 events of the type $K^-p \to \Lambda$ + neutrals was obtained in the Berkeley 25-inch hydrogen bubble chamber. In Section II we describe the experimental procedures and the bias corrections applied to the data. In Section III a qualitative description of the data is given. At the low momenta considered here there is appreciable overlap of the $\Sigma^0\pi^0$ and $\Lambda\pi^0$ contributions to the observed missing neutral mass spectrum. Contributions to the data from other final states (primarily $\Lambda\pi^0\pi^0$) further complicate the extraction of the cross sections and polarizations of the individual $\Sigma^0\pi^0$ and $\Lambda\pi^0$ final states. Section IV describes the event by event maximum likelihood fit used to extract Legendre polynomial expansion coefficients that describe the angular distributions and polarizations for the individual final states. Section V summarizes the results of this fit and presents our conclusions. The appendix explains the formulae used to derive the Σ^0 production distribution and polarization from those of its decay Λ.

II. EXPERIMENTAL PROCEDURES

From an exposure of the Berkeley 25-inch hydrogen bubble chamber to a K^- beam we have obtained 1.3×10^6 pictures. The beam has been fully described elsewhere.[4] Typically, each picture contained six K^- tracks and two background tracks. The background consisted of pions, muons, and some electrons. Background tracks had close to minimum ionization and were thus easily distinguished from the K^- tracks, which at our momentum have about three times minimum ionization.

By movement of the target and by use of a beryllium beam degrader, we were able to obtain K^- momenta between 240 and 450 MeV/c. The data were taken with 24 different beam settings. However, most of the path length (Fig. 1) occurs close to 395 MeV/c, the momentum required to form $\Lambda(1520)$.[5]

The film was scanned for all topologies including those with a zero prong and vee. On the basis of ionization, the scanners distinguished between vees from the decay $K^0 \to \pi^+\pi^-$ and those from the decay $\Lambda \to p\pi^0$. All of the film was scanned once; 38% was scanned twice; and 7% was scanned three times. All events within a restricted fiducial volume were measured with the Spiral Reader or Franckenstein measuring projectors. The kinematic reconstruction and fits to reaction hypotheses were performed with the programs TVGP and SQUAW. The vee for events scanned as $\overline{K}^0$ (Λ) was first fitted to the decay $\overline{K}^0 \to \pi^+\pi^-(\Lambda \to p\pi^0)$. The incident beam primary interaction point was used to determine the direction of the neutral making this a three constraint fit. If the fit to the decay failed then the opposite type vee was tried. If both failed then fits to three body $\overline{K}^0$ decays were tried. Those events which passed three

constraint decay fits were then fitted to the appropriate production and decay

$$K^- p \to \overline{K}^0 n \; ; \quad \overline{K}^0 \to \pi^+ \pi^- \tag{1}$$

$$K^- p \to \Lambda + \text{missing mass}; \quad \Lambda \to p\pi^0 \tag{2}$$

Events which failed to fit any reaction hypothesis were re-measured until 94% of those scanned as K^0 and 96% of those scanned as Λ passed. The remaining events were generally unmeasurable due to obscuration of a track or the presence of a very short track.

Of those events scanned as $\overline{K}^0$, 6.1% had a better confidence level for a fit to the Λ production and decay. Of those scanned as Λ, 1.4% had a better fit to the $\overline{K}^0$ production and decay.

Only those events which had a confidence level greater than 0.01 were accepted for further analysis. This sample included 29,109 events which fit only reaction (1); 70,815 events which fit only reaction (2); and 824 events which fit both reactions. Comparison of the confidence levels for those events fitting both reactions showed that in most cases one of the two fits was much preferred. An ambiguous event was considered to be the preferred reaction if the confidence level ratio for the fits was greater than 5.0. Re-examination of a sample of these events showed this to be a good criterion. Of the 824 events 82 were accepted as $\overline{K}^0$ events and 712 as Λ events. The remaining truly ambiguous 30 events, being a negligible number, were simply eliminated from the sample.

To ensure sufficient track lengths for a good measurement of the lambda momentum, further restrictions were made on the fiducial volumes for the production and decay vertices. These reduced the sample of Λ

events to 63,794 events. To correct for a scanning loss of shortlength lambdas, all events with a projected length less than 2.5 mm in space were eliminated and the remaining 57,880 events were weighted to account for the cut. The weighting also accounted for loss due to escape from the decay vertex fiducial volume. The mean weight was 1.23. Further losses were investigated by looking at the distribution of the decay proton in the lambda rest frame. Anisotropy in this distribution was found coming from the loss of events with shortlength protons and events with the lambda vee seen edge-on by the scanners. These biases were removed by rejecting events with a proton length less than 3 mm in space and weighting the remaining events. This reduced the sample to 56,748 events with a mean weight of 1.34.

The lifetime distribution of the final sample is shown in Fig. 2. In order to remove the effect of the cut on shortlength lambdas, the events have been plotted as a function of $(t - t_0)$ in units of the known lambda lifetime (τ_Λ). For each event, t_0 is given by 2.5 mm/$(\eta c\tau_\Lambda \cos\lambda)$, where η is the ratio of the lambda momentum to its mass and λ is the dip angle. This distribution is consistent with the line corresponding to the known lifetime ($\tau_\Lambda = 2.5 \times 10^{-10}$ sec). The depletion at large lifetimes comes from the escape of the lambdas from the chamber.

The cross section for the reaction was determined from a pathlength based on the tau decays of the beam. The analysis of these taus has been described in a previous publication.[6] The numbers of both taus and Λ + missing mass events were corrected for unobserved decay modes and for scanning efficiencies.

The scanning efficiencies were determined from the multiple scans

using an extension of the method developed by Derenzo and Hildebrand.[7] The analysis accounts for the differing visibility of events by parameterizing a visibility function $f(v)$, the fraction of the sample seen with an efficiency v, where v varies from 0.0 to 1.0. The extension used for this experiment defines a different visibility (v_1, v_2, and v_3) for each of the three scans to allow different efficiencies for each scan. The events found on each of the scans are fitted to determine the parameters of the function $f(v_1, v_2, v_3)$, which is then used to calculate the efficiencies. Details of this analysis can be found in Ref. 8. The overall scanning efficiency was 0.96.

III. DATA

The measured cross section for all Λ + neutrals is shown in Fig. 3. It falls from about 17 mb near 225 MeV/c to about 7 mb near 450 MeV/c. There is a 7 mb peak around 390 MeV/c from $\Lambda(1520)$. There are eight reactions which contribute to this cross section, the last three being negligible.

1. $K^- p \to \Lambda\pi^0$
2. $K^- p \to \Sigma^0\pi^0$, $\Sigma^0 \to \Lambda\gamma$
3. $K^- p \to \Lambda\pi^0\pi^0$
4. $K^- p \to \Lambda\gamma$
5. $K^- p \to \Sigma^0\gamma$, $\Sigma^0 \to \Lambda\gamma$
6. $K^- p \to \Lambda\pi^0\gamma$
7. $K^- p \to \Sigma^0\pi^0\gamma$, $\Sigma^0 \to \Lambda\gamma$
8. $K^- p \to \Sigma^0\pi^0\pi^0$, $\Sigma^0 \to \Lambda\gamma$

Since only the Λ in each of these final states is observed the data at each incident momentum yields a distribution in three variables:

i) μ^2, the invariant mass squared of the missing neutrals. This is related to the center of mass energy of the Λ as follows.

$$\mu^2 = E^2_{c.m.} - 2 E_{c.m.} E_\Lambda + m^2_\Lambda$$

ii) $\cos\theta$, the cosine of the angle between the missing mass and the K^- in the K^-p center of mass.

iii) $\cos\beta$, the cosine of the angle between the decay proton of the Λ and the normal to the missing mass production plane.

$$\cos\beta = \frac{\hat{p} \cdot (\vec{K} \times \vec{\mu})}{|\vec{K} \times \vec{\mu}|}$$

where $\vec{K}$ and $\vec{\mu}$ are the beam and missing mass directions and the unit vector $\hat{p}$ is the proton direction in the Λ rest frame.

A schematic diagram of the distributions in the invariant mass squared, μ^2, expected from the above reactions at 395 MeV/c incident momentum is shown in Fig. 4. The relative normalizations here are arbitrary and perfect mass resolution has been assumed. The $\Lambda\pi^0$ and $\Lambda\gamma$ final states contribute at single missing masses. It can be shown that the $\Sigma^0\pi^0$ and $\Sigma^0\gamma$ final states contribute rectangular distributions with upper and lower limits that vary slowly with incident momentum. The three body final states are illustrated as smooth distributions corresponding to projections of uniformly populated Dalitz plots.

Measurement errors naturally lead to finite resolution and an example of the measured missing mass distribution is shown in Fig. 5. Here the data for all values of $\cos\theta$ and $\cos\beta$ are plotted for the incident momentum interval 390 to 400 MeV/c. The program SQUAW calculates

an error for μ^2 for each event, $\delta(\mu^2)$, and this error has been used in the fits described below. The size of this error depends strongly on whether the proton comes to rest and its momentum is determined from range, or whether it leaves the chamber and its momentum is determined from curvature. Those events for which the proton momentum was determined from range have $\delta(\mu^2)$ between 0.06 and 0.20 in units of $m^2_{\pi^0}$. If the proton momentum was determined from curvature, then $\delta(\mu^2)$ ranges from 0.1 to 1.0 depending on the length of the track. Since $\delta(\mu^2)$ depends on the length of the proton track available for measurement, it is a function of both the energy (and therefore μ^2) and the production cosine of the Λ.

The variation of $\delta(\mu^2)$ and the different production distributions of the different reactions lead to very different mass spectra for various production angles. Figure 6 shows mass spectra for the data in the incident momentum interval 390 to 400 MeV/c for six bins of production cosine. The curves are from the fits described below.

IV. FITS TO THE DATA

In order to determine cross sections, angular distributions and polarizations for the $\Sigma^0\pi^0$ and $\Lambda\pi^0$ final states a maximum likelihood fit was made. The data were divided into intervals of 10 MeV/c and the data in each interval were fitted independently. The probability for each event was written as the sum of probabilities that the event was produced in one of the reactions above.

$$P(\mu_i^2, \cos\theta_i, \cos\beta_i) = p_{\Lambda\pi^0} + p_{\Sigma^0\pi^0} + p_{\Lambda\pi^0\pi^0} + \ldots.$$

We now describe the expressions used for each of these probabilities. A Gaussian resolution function has been used to account for the finite resolution in μ^2,

$$R(\mu^2, \mu'^2) = \frac{1}{\sqrt{2\pi}\,\delta(\mu^2)} \exp\left[-\frac{1}{2}\left(\frac{\mu^2 - \mu'^2}{\delta(\mu^2)}\right)^2\right]$$

where the Gaussian width used for each event was the $\delta(\mu^2)$ calculated by SQUAW. The angular distributions and polarizations for the $\Sigma^0\pi^0$ and $\Lambda\pi^0$ have been expanded through $\ell = 4$.

The probability for the $\Lambda\pi^0$ final state

$$P_{\Lambda\pi^0}(\mu^2, \cos\theta, \cos\beta) = f_{\Lambda\pi}\, R(\mu^2, m_\pi^2) \times$$
$$\sum_{\ell=0}^{4}\left[\frac{A_\ell}{A_0} P_\ell(\cos\theta) + \alpha_\Lambda \cos\beta \sin\theta \frac{B_\ell}{A_0} P'_\ell(\cos\theta)\right]$$

where the Λ decay asymmetry parameter, $\alpha = 0.645$ (Ref. 9). The parameter $f_{\Lambda\pi}$ is the fraction of the Λ + neutral events coming from $\Lambda\pi^0$ production. This fraction along with the A_ℓ/A_0 and B_ℓ/B_0 are varied in the fit.

The probability for the $\Sigma^0\pi^0$ final state

$$P_{\Sigma^0\pi^0}(\mu^2, \cos\theta, \cos\beta) = f_{\Sigma\pi}\int_{\mu^2_{min}}^{\mu^2_{max}} R(\mu^2, \mu'^2) \times$$
$$\sum_{\ell=0}^{4}\left[\frac{A_\ell}{A_0} U_\ell(\mu'^2)\, P_\ell(\cos\theta) + \alpha_\Lambda \cos\beta \sin\theta \frac{B_\ell}{A_0} V_\ell(\mu'^2)\, P'_\ell(\cos\theta)\right] d\mu'^2$$

The functions U_ℓ and V_ℓ account for the spreading of the distribution due

to decay of the Σ^0 into $\Lambda\gamma$. The form of these functions are described in the appendix. The computer code of this prescription for unfolding the Λ angular distribution and polarization to derive the Σ^0 angular distribution and polarization was tested to better than 1% using Monte-Carlo generated events. The coefficients A_ℓ and B_ℓ, describing the $\Sigma^0\pi^0$ angular distribution and polarization in the K^-p rest frame, along with the fraction $f_{\Sigma\pi}$ are varied in the fits.

The probability for the $\Lambda\pi^0\pi^0$ final state

$$P_{\Lambda\pi\pi}(\mu^2,\cos\theta,\cos\beta) = f_{\Lambda\pi\pi}\int g(\mu'^2,\cos\theta,\cos\beta)\, R(\mu^2,\mu'^2)\, d\mu'^2 \ .$$

Only the fraction $f_{\Lambda\pi\pi}$ was varied in the fitting. The function g has been calculated from the results of a detailed analysis of the related channel $\Lambda\pi^+\pi^-$. An isobar model partial wave analysis has been made of 9200 $\Lambda\pi^+\pi^-$ events from the same exposure and the results have been published.[2] A good fit to the $\Lambda\pi^+\pi^-$ events was obtained with only six isobar amplitudes. The channel is dominated by $I = 0$ production of $\Sigma(1385)$ corresponding to the sequence $K^-p \to \Lambda(1520) \to \Sigma(1385)\ \pi \to \Lambda\pi^+\pi^-$; the isospin 1 production is very small. The $I = 0$ amplitudes found in the $\Lambda\pi^+\pi^-$ analysis contribute to $\Lambda\pi^0\pi^0$ and have been used to calculate the function g. The appropriate changes due to the $\pi^\pm - \pi^0$ mass difference were made.

The probability for the $\Lambda\gamma$ final state

$$P_{\Lambda\gamma}(\mu^2,\cos\theta,\cos\beta) = f_{\Lambda\gamma}\, R(\mu^2,0)\left[1-\frac{1}{2}P_2(\cos\theta)\right]$$

A study of the reaction $K^- p \to \Lambda\gamma$ has been made from this same exposure.[10] By isolating a sample of events well resolved in μ^2 the cross section and angular distribution for the reaction were measured. The cross section peaks at 395 MeV/c indicating dominance of $\Lambda(1520)$ production and the angular distribution is consistent with $1 - \frac{1}{2} P_2(\cos\theta)$, expected from the electric dipole decay of $\Lambda(1520)$. In the fitting here both the angular distribution and the fraction $f_{\Lambda\gamma}$ were fixed. At 395 MeV/c the $\Lambda\gamma$ channel accounts for 2.4% of the Λ + neutral cross section.

$$P_{\Sigma^0\gamma} = 3.0\,\rho\, f_{\Lambda\gamma} \int_{\mu^2_{min}}^{\mu^2_{max}} R(\mu^2,\mu'^2)\, d\mu'^2 \left[1 - \frac{1}{2} P_2(\cos\theta)\right]$$

To describe the $\Sigma^0\gamma$ we have assumed all the $\Lambda\gamma$ comes from $\Lambda(1520)$ and then used U-spin conservation to calculate $\Sigma^0\gamma$. U-spin in variance gives a factor 3 in cross section, ρ is the ratio of phase space (about 0.85), and we have neglected the spreading of the angular distribution from the Σ^0 decay. At 395 MeV/c, $\Sigma^0\gamma$ accounts for 6.2% of the Λ + neutrals cross section.

There is no direct way to measure the $\Lambda\pi\gamma$ and $\Sigma^0\pi^0\gamma$ contributions here. Estimates made on the basis of phase space arguments and SU(3) however, indicate they contribute about 0.1% of the cross section. We have neglected these in the fitting.

An analysis of the $\Sigma^+\pi^-\pi^0$, and $\Sigma^0\pi^+\pi^-$ final states have been made from data from this same exposure.[2] That analysis showed the $\Sigma\pi\pi$ final states were dominated by $\Lambda(1520)$ production and were consistent with the decay sequence $\Lambda(1520) \to \Sigma(1385)\ \pi \to \Sigma\pi\pi$. However, isospin conservation

prohibits the $\Sigma^0\pi^0\pi^0$ final state from this sequence. A small amount of $\Sigma\pi\pi$ phase space was found in the charged channels and this leads to an estimate of 0.2% $\Sigma^0\pi^0\pi^0$ in the Λ + neutral near 400 MeV/c incident momentum. We have neglected this in the fitting.

The variables μ^2 and $\delta(\mu^2)$ from SIOUX have been altered slightly before fitting the data. In the raw data a systematic shift in the mass of the π^0 peak was observed. Such a shift can arise from small systematic errors in the beam momentum, the fitted energy of the Λ, and the production angle of the Λ. We have corrected the data with a phenomenological shift which varied from $-0.08\ m^2_{\pi^0}$ at $\cos\theta = 0.0$ to 0.0 at $\cos\theta = \pm 1.0$. Introduction of this shift changed the fractions by ≤ 0.004 and the Legendre coefficients by less than 1/2 standard deviation. The error $\delta(\mu^2)$ was scaled by a factor f_s for events with stopping protons and f_ℓ for events with leaving protons. Variation of these scaling factors made a small improvement in the likelihood. The final fitting was made with $f_s = 1.2$ and $f_\ell = 1.0$. Inclusion of these scaling factors changed the Legendre coefficients by an average of 0.1 standard deviations and the fractions by 0.003.

Using the above expressions, a likelihood fit to the data was made using the OPTIME system.[11] The Legendre expansion coefficients and the fractions $f_{\Lambda\pi}$, $f_{\Sigma\pi}$, and $f_{\Lambda\pi\pi}$ were varied in the fits. Monte Carlo events with the same distribution of errors were used to plot the fits over the data for comparison. The curves resulting from the fit at 395 MeV are shown in Fig. 6(a) to (f). The data has been broken into six bins of lambda production cosine. The contributions from the individual channels as well as the total are drawn. The fits correctly reproduce the variations

with incident momentum and production cosine.

The cross sections and coefficients from these fits were then corrected to take into account a systematic error introduced by beam averaging the individual events in SQUAW. For each of the 24 beam settings an average beam momentum was established from the taus and this average momentum was averaged with the measured momentum of the K^- track before kinematic fitting. This beam averaging procedure was done for both the Λ events and the taus used to determine the pathlength. Since the taus (3 constraint) were better constrained than the Λ's (0 constraint), the distribution in momentum for the Λ's was pulled closer to the average. This had the effect of artificially raising the cross section for momenta in the center of the distribution and lowering it on the sides. This artifact became apparent in comparing the cross sections from events from different beam settings. The experiment of Berley et al., that measured these channels in this momentum region also found cross sections and coefficients from different runs to be inconsistent (see Figs. 3, 7 - 10). Using the known beam averaging procedure and the known error distributions, we derived an algorithm for correcting the cross sections and Legendre coefficients.[12] The algorithm also included an unfolding of the uncertainty in the beam momentum. The algorithm was applied to the data and the resulting cross sections from different beam settings agreed well. The changes in the final cross sections averaged about one standard deviation and the changes in the coefficients averaged much less than a standard deviation. All of the results described in the following section have been corrected.

V. RESULTS

The fractions $f_{\Lambda\pi}$, $f_{\Sigma\pi}$, and $f_{\Lambda\pi\pi}$ from the fits have been combined with the cross sections for all Λ + neutrals to derive the partial cross sections shown in Table 1 and Fig. 3(b), (c) and (d). The three cross sections are strongly correlated and only the diagonal errors are given in the table and the figures.

The $\Lambda\pi^0$ cross section [Fig. 3(b)] falls smoothly from about 10 mb at 245 MeV/c to about 3 mb at 445 MeV/c. Our data fall systematically below those of Berley et al.[13] and slightly above those of Watson et al.[1] in the region near $\Lambda(1520)$. At the upper end, our data connect smoothly with the results of Armenteros, et al.[14] The $\Lambda(1520)$ has I = 0 and the lack of structure near 400 MeV/c in this pure I = 1 channel is evidence that the procedure described above has cleanly separated the final states.

The $\Sigma^0\pi^0$ cross section [Fig. 3(c)] shows a marked peak from the $\Lambda(1520)$ of about 4 mb above a 3 mb background. There is no other significant structure. Again our data are systematically below those of Berley et al. and join smoothly with those of Armenteros, et al.

The $\Lambda\pi^0\pi^0$ cross sections (shown as full circles in Fig. 3(d)) rises rapidly from zero to 1.7 mb and then falls to about 1.0 mb. Although the form of the $\Lambda\pi^0\pi^0$ mass spectra and angular distributions were fixed in the fitting, the amount of this channel was freely chosen by the fit. Isotopic spin invariance predicts the $\Lambda\pi^0\pi^0$ cross section is 1/2 of the $\Lambda\pi^+\pi^-$ cross section, since the latter is almost pure I = 0.[2] Figure 3(d) shows as vertical lines the measured $\Lambda\pi^+\pi^-$ cross sections multiplied by 2ρ, where ρ is the ratio of available phase space. The excellent agreement

is an additional consistency check on the separation of the different final states.

The Legendre coefficients for the $\Lambda\pi^0$ angular distribution and polarization are shown in Figs. 7 and 8 and Table II. Only the diagonal errors are shown. The A_1/A_0 is in agreement with both Berley et al. and Armenteros et al., while the A_2/A_0 coefficient is in agreement with Berley and falls below the results of Armenteros at the upper end. A_3/A_0 is slightly positive and A_4/A_0 is consistent with zero. The B_1/A_0 and B_2/A_0 are both significantly non-zero and positive throughout this region and in agreement with the previous experiments[13,14] B_3/A_0 and B_4/A_0 are consistent with zero.

The Legendre coefficients for the $\Sigma^0\pi^0$ angular distributions and polarizations are shown in Table III and Figs. 9 and 10. Both the A's and B's show dramatic behavior from the $\Lambda(1520)$ D-wave and its interference with the dominant S-wave background. The data of Berley et al. show considerably less A_2/A_0 than our own. The dramatic structure seen in the A_2/A_0 is not observed in the A_2/A_0 for the $\Lambda\pi^0$ channel indicating again the clean separation of the channels.

The differential cross sections for π^0 production at 0° and 180° in the reactions $\Lambda\pi^0$ and $\Sigma^0\pi^0$ can be calculated from the Legendre coefficients and the total cross sections. These are displayed as a function of momentum in Fig. 11. Uncertainties are calculated using the full error matrix. The spectacular rise and fall of the $\Sigma^0\pi^0$ cross section in the vicinity of 390 MeV/c both at 0° and 180° is observed only slightly, if at all, in $\Lambda\pi^0$. Neither for forward produced Λ, where the missing mass is poorly measured, nor for backward produced Λ is there any evidence for

more than a few percent contamination from $\Sigma^0\pi^0$, indicating once again the clean separation of these channels. Alternatively, any effect seen could also be ascribed to isospin impurity once suggested by Dalitz and Von Hippel[15] and investigated by Berley et al.[13]

Below 350 MeV/c the $\Sigma^0\pi^0$ cross sections in the forward and backward directions behave erratically, fluctuating well outside of their statistical uncertainty. We have no explanation for this. Perhaps it comes from the paucity of events below 350 MeV/c, inadequate for the elaborate parameterization. The $\Lambda\pi^0$ cross sections show no significant evidence for structure. Interest in the region near 280 MeV/c incident momentum has been generated by an enhancement seen by Pan and Forman[16] in the reaction $\pi^+p \to K^+\pi^+\Lambda$. On the basis of an enhancement seen in the $\Lambda\pi^+$ mass distribution and structure in the polarization, they suggest an isotopic spin 1 resonance with mass = 1480 ± 15 MeV and width = 35 ± 20 MeV. Cline, Laumann, and Mapp[17] also suggest the possibility of a resonance with this mass. They observe in this energy region rapid variations in Legendre coefficients which describe the $\Lambda\pi^-$ angular distribution in the reaction $K^-d \to \Lambda\pi^-p$. However, the complications introduced by the three particle final state in both these experiments makes a clean resonance interpretation of these effects difficult. In our experiment we find no evidence for a resonance at 1480 MeV. If a resonance of mass and width given by Ref. 16 were to have as much as 5% coupling to the $\bar{K}N$ channel, and were to decay dominantly via $\Lambda\pi^0$, then we would have observed a $3.7(J+\frac{1}{2})$ mb enhancement in the $\Lambda\pi^0$ cross section centered at 280 MeV/c with a full width of 100 MeV/c. A coupling this large to the elastic channel seems to be ruled out by the data displayed in Fig. 3(b).

Table I. Cross sections and errors (mb) for Λ + missing neutrals, $\Lambda\pi^0$, $\Sigma^0\pi^0$, and $\Lambda\pi^0\pi^0$ final states.

Momentum (MeV/c)	$\sigma(\Lambda$ + neutrals)		$\sigma(\Lambda\pi^0)$		$\sigma(\Sigma^0\pi^0)$		$\sigma(\Lambda\pi^0\pi^0)$	
225	15.98	2.84						
235	12.78	1.60						
245	18.42	1.60	10.23	1.06	8.18	0.92		
255	16.50	1.14	8.82	0.74	7.68	0.68		
265	13.88	0.86	7.77	0.58	6.11	0.50		
275	14.77	0.85	8.04	0.56	6.73	0.50		
285	11.16	0.63	5.56	0.40	5.61	0.40		
295	12.47	0.71	6.69	0.47	5.78	0.43		
305	11.85	0.67	6.35	0.45	5.49	0.41		
315	9.91	0.60	5.29	0.40	4.37	0.36	0.21	0.36
325	10.09	0.56	5.41	0.37	4.48	0.33	0.14	0.32
335	9.69	0.53	5.22	0.34	4.11	0.30	0.26	0.29
345	9.81	0.52	4.78	0.33	4.77	0.33	0.10	0.37
355	9.61	0.33	4.86	0.21	4.15	0.19	0.33	0.19
365	10.08	0.25	4.21	0.13	4.86	0.15	0.54	0.13
375	12.53	0.24	4.29	0.11	6.45	0.15	0.97	0.12
385	15.27	0.25	4.20	0.10	8.30	0.15	1.53	0.13
395	15.03	0.27	3.96	0.11	8.10	0.16	1.66	0.14
405	13.14	0.30	3.90	0.12	6.72	0.17	1.52	0.15
415	11.71	0.29	3.87	0.14	5.93	0.18	1.20	0.17
425	10.84	0.36	4.05	0.20	5.17	0.22	1.10	0.23
435	7.57	0.41	3.49	0.26	2.97	0.24	0.71	0.26
445	8.11	0.54	3.45	0.31	3.26	0.30	1.08	0.32
455	9.25	0.71						
465	6.51	0.58						

Table II. Legendre polynomial coefficients A_ℓ/A_0 and B_ℓ/A_0 for $K^- p \to \Lambda\pi^0$.

Momentum (MeV/c)	A_1/A_0		A_2/A_0		A_3/A_0		A_4/A_0	
245	.953	.143	.309	.204	.241	.243	-.153	.279
255	.847	.111	.194	.163	.204	.190	.133	.199
265	.918	.104	.432	.146	.005	.163	.189	.180
275	.995	.091	.420	.137	.065	.159	.114	.168
285	1.148	.099	.767	.146	.261	.171	.336	.173
295	.938	.101	.617	.139	.304	.165	-.049	.167
305	1.143	.097	.292	.156	-.122	.184	-.072	.174
315	1.187	.111	.761	.171	.199	.199	.194	.189
325	1.160	.104	.903	.146	.404	.168	.047	.162
335	1.321	.081	.610	.142	.148	.163	.269	.157
345	1.154	.107	.569	.175	-.035	.206	.147	.196
355	1.141	.068	.609	.100	-.027	.120	.025	.115
365	1.195	.046	.567	.068	.109	.082	-.204	.079
375	1.254	.038	.523	.059	.125	.071	-.062	.067
385	1.311	.036	.536	.055	.038	.067	-.023	.065
395	1.372	.042	.658	.065	.185	.077	.094	.076
405	1.435	.042	.632	.069	.280	.082	-.007	.077
415	1.427	.061	.679	.097	.095	.116	-.082	.109
425	1.267	.101	.583	.148	.037	.181	-.268	.176
435	1.306	.108	.409	.190	.169	.216	.013	.213
445	1.202	.110	.372	.183	-.195	.218	.062	.216

Momentum (MeV/c)	B_1/A_0		B_2/A_0		B_3/A_0		B_4/A_0	
245	.531	.241	.043	.204	.027	.172	.074	.135
255	.261	.211	-.008	.166	-.148	.140	-.278	.117
265	.342	.173	.062	.149	-.175	.134	-.079	.104
275	.310	.160	.171	.134	.099	.113	.053	.088
285	.021	.166	-.213	.140	-.162	.117	-.151	.099
295	.070	.165	.032	.139	.105	.116	.138	.098
305	.454	.175	.232	.145	-.042	.124	-.058	.100
315	.412	.193	.103	.170	-.090	.148	-.034	.107
325	.143	.172	-.030	.169	-.123	.149	-.019	.105
335	.097	.155	.047	.128	.012	.116	.084	.083
345	-.050	.184	-.096	.156	-.231	.128	-.119	.110
355	-.000	.116	.134	.099	-.043	.084	.043	.065
365	.132	.079	.158	.068	-.022	.059	-.023	.046
375	.037	.068	.108	.058	-.057	.050	-.041	.038
385	.152	.060	.098	.052	-.023	.045	-.044	.035
395	.246	.068	.203	.059	.063	.050	-.002	.041
405	.125	.073	.174	.063	.084	.054	-.048	.042
415	.053	.102	-.077	.089	-.073	.075	-.028	.057
425	.288	.167	.211	.145	-.087	.122	.002	.092
435	.254	.185	.128	.156	-.005	.137	-.139	.099
445	.186	.205	.104	.166	-.070	.141	-.261	.106

Table III. Legendre polynomial coefficients A_ℓ/A_0 and B_ℓ/A_0 for $K^- p \to \Sigma^0 \pi^0$.

Momentum (MeV/c)	A_1/A_0		A_2/A_0		A_3/A_0		A_4/A_0	
245	-.313	.173	-.215	.253	-.398	.350	.251	.488
255	-.293	.138	-.218	.193	.396	.263	-.373	.395
265	-.248	.118	-.379	.174	-.283	.226	.116	.287
275	-.205	.108	-.260	.155	-.087	.216	-.135	.325
285	-.286	.105	-.085	.148	-.211	.204	-.115	.292
295	-.099	.124	-.317	.181	.133	.263	-.370	.368
305	-.211	.126	-.195	.185	.010	.243	.146	.340
315	-.074	.149	.039	.210	.482	.267	-.156	.365
325	-.346	.100	-.535	.138	-.018	.203	-.406	.303
335	-.090	.097	-.580	.129	-.131	.186	-.516	.255
345	-.178	.123	-.064	.175	.270	.228	.471	.295
355	-.234	.077	-.249	.107	.055	.138	-.163	.185
365	-.317	.046	.281	.064	.236	.083	-.008	.110
375	-.354	.039	.551	.050	.222	.064	-.040	.087
385	-.248	.035	1.315	.040	.113	.054	.037	.072
395	-.187	.042	1.781	.046	-.074	.063	-.050	.084
405	-.135	.046	1.877	.050	-.283	.068	.023	.088
415	-.066	.072	1.859	.079	-.344	.110	.120	.138
425	.027	.124	1.690	.133	-.608	.180	-.630	.246
435	-.245	.179	1.747	.199	-.652	.268	.321	.341
445	.029	.149	.697	.184	-.203	.254	-.633	.306

Momentum (MeV/c)	B_1/A_0		B_2/A_0		B_3/A_0		B_4/A_0	
245	.969	.853	-.418	.695	.415	.600	-.203	.570
255	.264	.641	-.324	.536	.458	.530	.262	.523
265	.428	.601	.433	.483	.042	.461	-.892	.468
275	.323	.535	-.376	.428	-.001	.383	.126	.384
285	.850	.500	-.290	.383	-.007	.334	-.125	.349
295	-.632	.536	-.098	.417	-.453	.395	.489	.383
305	.357	.623	.176	.473	.686	.437	-.223	.443
315	-.232	.571	-.344	.458	-.421	.419	-.024	.472
325	.604	.549	-.056	.407	-.161	.354	.556	.319
335	-.076	.508	-.532	.379	-.257	.331	-.172	.341
345	.963	.507	-.569	.417	.083	.392	-.054	.397
355	.815	.370	-.367	.290	-.491	.256	.064	.258
365	.467	.205	-.863	.160	-.094	.144	-.135	.146
375	.095	.145	-.853	.123	-.022	.112	-.126	.110
385	.341	.108	-.664	.103	.348	.089	-.033	.089
395	.082	.120	-.564	.121	.220	.101	-.009	.101
405	.298	.135	-.086	.139	.261	.115	.099	.109
415	.190	.203	-.018	.209	.342	.170	-.136	.169
425	.518	.352	.743	.377	.376	.310	.257	.274
435	.750	.504	.346	.534	-.062	.449	-.032	.416
445	.816	.550	.286	.496	.660	.400	-.560	.418

APPENDIX

In the reaction $K^- p \to \Sigma^0 \pi^0$, $\Sigma^0 \to \Lambda\gamma$ the angular distributions and polarization of the Λ can be measured and described in terms of Legendre polynomial expansions. In this appendix we describe the formulae used to relate the measured Legendre coefficients for the Λ to those describing the angular distribution and polarization of the Σ^0.

The relations used here are based on the work of Cha and Sucher.[18] We have converted their general expressions to relations between Legendre polynomial expansion coefficients.

Table A1 and Fig. A1 define the notation used. Cha and Sucher derive the following distribution for the Λ (Eq. 2.14).

$$\frac{d\sigma}{dE_\Lambda \, d\cos\theta_\Lambda} = \frac{1}{2\pi(E_\Lambda^+ - E_\Lambda^-)} \int_0^{2\pi} \frac{d\sigma}{d\cos\gamma} \, d\phi \ . \tag{A1}$$

Expanding the production angular distribution we write

$$\frac{d\sigma}{d\cos\gamma} = \sum_{\ell=0}^{\infty} A_\ell P_\ell(\cos\gamma) \ . \tag{A2}$$

Using the vector addition theorem, $P_\ell(\cos\gamma)$ can be expressed

$$P_\ell(\cos\gamma) = P_\ell(\cos\chi)\, P_\ell(\cos\theta_\Lambda) + 2\sum_{m=1}^{\ell} \frac{(\ell-m)!}{(\ell+m)!} P_\ell^m(\cos\chi) P_\ell^m(\cos\theta_\Lambda) \cos m\phi \ . \tag{A3}$$

The integral over ϕ of the second term vanishes yielding

$$\frac{d\sigma}{dE_\Lambda \, d\cos\theta_\Lambda} = \frac{1}{(E_\Lambda^+ - E_\Lambda^-)} \sum_{\ell=0}^{\infty} A_\ell P_\ell(\cos\chi) \; P_\ell(\cos\theta_\Lambda) \quad . \tag{A4}$$

$\cos\chi$ is related to the energies of the Σ and Λ by

$$\cos\chi = \frac{2E_\Lambda E_\Sigma - m_\Sigma^2 - m_\Lambda^2}{2|p_\Sigma| \; |p_\Lambda|} \tag{A5}$$

The missing neutral mass is given by

$$\mu^2 = E_{c.m.} - 2E_{c.m.} \; E_\Lambda + m_\Lambda^2 \quad ,$$

and the differential cross section for the Λ becomes

$$\frac{d\sigma}{d\mu^2 \, d\cos\theta_\Lambda} = \frac{1}{\mu^2_{max} - \mu^2_{min}} \sum_{\ell=0}^{\infty} A_\ell P_\ell(\cos\chi) \; P_\ell(\cos\theta_\Lambda)$$

or

$$\frac{d\sigma}{d\mu^2 \, d\cos\theta_\Lambda} = \sum_{\ell=0}^{\infty} A_\ell U'_\ell(\mu^2) \; P_\ell(\cos\theta_\Lambda) \tag{A6}$$

where

$$U_\ell(\mu^2) = \frac{1}{\mu^2_{max} - \mu^2_{min}} P_\ell(\cos\chi) \tag{A7}$$

Cha and Sucher's result relating the polarization of the Λ to that of the Σ^0 is the following.

$$\eta_\Lambda(\theta_\Lambda,E) = 2\pi \sin\theta_\Lambda \xi_\Lambda \Big/ \int_0^{2\pi} \frac{d\sigma}{d\cos\gamma}\, d\phi$$

where $$\xi_\Lambda = \frac{1}{2\pi}\alpha_0 |\vec{p}_\Lambda| |\vec{p}_\Sigma| \sin^2\chi \int_0^{2\pi} \xi_\Sigma(\cos\gamma) \sin^2\phi \, d\phi \qquad \text{(A8)}$$

η_Λ is the polarization of the Λ in the direction

$$\frac{\vec{p}_K \times \vec{p}_\Lambda}{|\vec{p}_K \times \vec{p}_\Lambda|} \quad \text{and} \quad \alpha_0 = \frac{-4m_\Sigma m_\Lambda}{(m_\Sigma - m_\Lambda)^2}$$

ξ_Σ is related to the polarization of the Σ^0, η_Σ, by

$$\eta_\Sigma = \sin\theta_\Sigma \xi_\Sigma \Big/ \frac{d\sigma}{d\cos\gamma} \, . \qquad \text{(A9)}$$

We expand IP for the Σ^0 as follows

$$IP = \frac{d\sigma}{d\cos\gamma}\eta_\Sigma = \sin\gamma \sum_{\ell=1}^{\infty} B_\ell P'_\ell(\cos\gamma) \, . \qquad \text{(A10)}$$

Thus

$$\eta_\Lambda(\theta_\Lambda,E_\Lambda) = \sin\theta_\Lambda \alpha_0 |\vec{p}_\Lambda| |\vec{p}_\Sigma| \sin^2\chi \sum_{\ell=1}^{\infty} B_\ell I_\ell \Big/ \int_0^{2\pi} \frac{d\gamma}{d\cos\gamma}\, d\phi \, ,$$

where $$I_\ell = \int_0^{2\pi} P_\ell(\cos\gamma) \sin^2\phi \, d\phi \, . \qquad \text{(A11)}$$

Now, using the relation

$$\cos\gamma = \cos\chi \cos\theta_\Lambda - \sin\chi \sin\theta_\Lambda \cos\phi \tag{A12}$$

and an integration by parts, I_ℓ may be re-expressed

$$I_\ell = -\int_0^{2\pi} \frac{P_\ell(\cos\gamma) \cos\phi \, d\phi}{\sin\theta_\Lambda \sin\chi}$$

Application of the vector addition addition theorem yields

$$I_\ell = 2\pi \frac{(\ell - 1)!}{(\ell + 1)!} P'_\ell(\cos\theta_\Lambda) P'_\ell(\cos\chi) \quad . \tag{A13}$$

Now, with relations (A6), (A7), (A11), and (A13) for the angular distributions and polarization we can express the measured distribution as follows

$$\frac{d\sigma}{d\mu^2 \, d\cos\theta_\Lambda \, d\cos\beta_\Lambda} = \sum_{\ell=0}^{\infty} A_\ell U_\ell P_\ell(\cos\theta_\Lambda) + \alpha_\Lambda \cos\beta \sin\theta_\Lambda \sum_{\ell=1}^{\infty} B_\ell V_\ell P'_\ell(\cos\theta_\Lambda) \tag{A14}$$

where $$U = \frac{1}{\mu^2_{max} - \mu^2_{min}} P_\ell(\cos\chi) \tag{A15}$$

and $$V_\ell = \frac{2\pi}{\mu^2_{max} - \mu^2_{min}} \sin\theta_\Lambda \, \alpha_0 |\vec{p}_\Lambda| \, |\vec{p}_\Sigma| \sin^2\chi \frac{P'_\ell(\cos\chi)}{\ell(\ell+1)} \tag{A16}$$

α_Λ is the Λ decay asymmetry parameter and β is the angle between the Λ and the decay proton in the Λ rest frame.

These expressions for U_ℓ and V_ℓ can be integrated over the full range of μ^2 to give factors describing the smearing of the Σ^0 distribution (for all μ^2) by the decay. These integrals have been performed numerically and the results are shown in Table AII for incident K^- momenta from 275 to 465 MeV/c.

Table AI. Notation used in the description of $K^-p \to \Sigma^0\pi^0$, $\Sigma^0 \to \Lambda\gamma$. All quantities listed here are defined in the K^-p center of mass. The Λ momentum is chosen along the z-axis and the beam is chosen in the x-z plane. See Fig. A1.

θ_Λ	the polar angle of the beam with respect to the Λ
χ ϕ	the polar and azimuthal angles of the Σ^0 with respect to the Λ
γ	the angle between the Σ^0 and the K^-
E_Λ, P_Λ	the energy and momentum of the Λ
E_Σ, p_Σ	the energy and momentum of the Σ^0
E_Λ^+, E_Λ^-	the maximum and minimum possible energy of the Λ

Table AII. Integrals of U_ℓ and V_ℓ over all missing mass. U_ℓ and V_ℓ are factors relating the Legendre coefficients which describe the angular distribution and polarization of the Σ^0 to those of the measured Λ.

Incident K^- mom. (MeV/c)	U_ℓ				V_ℓ			
	$\ell = 1$	2	3	4	1	2	3	4
305	0.962	0.890	0.787	0.661	0.325	0.311	0.290	0.263
345	0.966	0.901	0.807	0.692	0.326	0.313	0.294	0.270
385	0.970	0.910	0.826	0.720	0.327	0.315	0.298	0.276
425	0.973	0.919	0.842	0.746	0.327	0.317	0.301	0.281
465	0.975	0.927	0.857	0.768	0.328	0.318	0.304	0.286

FOOTNOTES AND REFERENCES

*This work was performed under the auspices of the U. S. Atomic Energy Commission.

1. M. B. Watson, M. Ferro-Luzzi, and R. D. Tripp, Phys. Rev. 131, 2248-2281 (1963).
2. Analyses of the $\Lambda\pi^+\pi^-$ and $\Sigma\pi\pi$ final states have been published in Physical Review D 7, 5 (1973) and Physical Review D 7, 3212 (1973). Analyses of the $\Sigma^{\pm}\pi^{\mp}$ and $\bar{K}N$ final states are in progress.
3. R. Bangerter, T. Mast, and R. Tripp (to be published).
4. R. O. Bangerter, K-65 Beam Optics, Lawrence Berkeley Laboratory, Alvarez Group Physics Note No. 574, October 1965 (unpublished).
5. Most of the pathlength below 300 MeV/c is derived from an exposure of the 25-inch hydrogen bubble chamber to the same beam by Chan and Kadyk (see J. H. Chan, Lawrence Berkeley Laboratory Report LBL-350) (1971).
6. T. S. Mast, L. K. Gershwin, M. Alston-Garnjost, R. O. Bangerter, A. Barbaro-Galtieri, J. J. Murray, F. T. Solmitz, and R. D. Tripp, Phys. Rev. 183, 1200 (1969).
7. S. E. Derenzo and R. H. Hildebrand, The Estimation of Scanning Efficiencies for Experiments Using Visual Detectors, Lawrence Berkeley Laboratory Report UCRL-18638 (1968).
8. R. Bangerter and T. Mast, Scan Efficiencies from Multiple Scans, Lawrence Berkeley Laboratory Alvarez Group Physics Note No. 731, October 1971 (unpublished).
9. Particle Data Group, Reviews of Mod. Phys. 43, 2, Part II (April 1971).

10. T. S. Mast, M. Alston-Garnjost, R. O. Bangerter, A. Barbaro-Galtieri, L. K. Gershwin, F. T. Solmitz and R. D. Tripp, Phys. Rev. Letters 21, 1715 (1968).

11. P. H. Eberhard and W. O. Koellner, The Optime System for Fitting Theoretical Expressions and Users Manual for the Optime System, Lawrence Berkeley Laboratory Reports UCRL-20159 (1970) and UCRL-20160 (1971).

12. R. Bangerter, Alvarez Group Physics Note (unpublished).

13. D. Berley, S. P. Yamin, R. R. Kofler, A. Mann, G. W. Meisner, S. S. Yamamoto, J. J. Thompson, and W. Willis, Physical Review D 1, 1996 (1970).

14. R. Armenteros, P. Baillon, C. Briceman, M. Ferro-Luzzi, E. Pagiola, J. O. Petersen, D. E. Plane, N. Schmitz, E. Burkhardt, H. Filthuth, E. Kluge, H. Oberlack, R. R. Ross, R. Barloutaud, P. Granet, J. Meyer, J. P. Porte, and J. Prevost, Nucl. Phys. B21, 15-76 (1970).

15. R. H. Dalitz and F. Von Hippel, Phys. Letters 10, 153 (1964).

16. Y. Pan and F. Forman, Phys. Rev. Letters 23, 806 (1969).

17. D. Cline, R. Laumann, and J. Mapp, Letters al Nuovo Cimento. 6, 205 (1972).

18. M. H. Cha and J. Sucher, Phys. Rev. 140, 668 (1965).

FIGURE CAPTIONS

Fig. 1. Pathlength (events/millibarn) versus incident K^- momentum (MeV/c).

Fig. 2. Distribution of Λ lifetimes shifted by the cut imposed to remove the effect of the loss of short length Λ's. The depletion at large lifetimes comes from the escape of the Λ's from the chamber.

Fig. 3. (a) Cross section (millibarns) for the reaction $K^-p \to \Lambda$ + missing neutrals as a function of incident K^- momentum (MeV/c). (b),(c), and (d) Cross sections (millibarns) for the $\Lambda\pi^0$, $\Sigma\pi^0$, and $\Lambda\pi^0\pi^0$ final states derived from the fits described in the test. The data of Berley, et al. (Ref. 13), Armenteros, et al. (Ref. 14), and Watson, et al. (Ref. 1) are shown for comparison. The data shown with vertical lines in Fig. 3(d) are predictions based on isotopic spin in variance and the $\Lambda\pi^+\pi^-$ cross sections measured from the same bubble chamber exposure.

Fig. 4. Schematic diagram of the distributions in missing mass squared expected from different final states at 395 MeV/c. The vertical scale and relative normalizations are arbitrary.

Fig. 5. Measured distribution of missing mass squared for events with incident momenta between 390 and 400 MeV/c.

Fig. 6. Distributions in missing mass squared for data in the incident momentum interval 390 to 400 MeV/c for six bins of production cosine. The curves are the contributions from different final states and the total derived from the fits described in the text.

Fig. 7. Legendre coefficients A_ℓ/A_0 (ℓ = 1, 4) as a function of incident momentum for the angular distribution in the reaction $K^-p \to \Lambda\pi^0$. The data of Berley, et al. (Ref. 13) and Armenteros, et al. (Ref. 14) are shown for comparison.

Fig. 8. Legendre coefficients B_ℓ/A_0 (ℓ = 1, 4) as a function of incident momentum for the Λ polarization in the reaction $K^-p \to \Lambda\pi^0$. The data of Berley, et al. (Ref. 13) and Armenteros, et al. (Ref. 14) are shown for comparison.

Fig. 9. Legendre coefficients A_ℓ/A_0 (ℓ = 1, 4) as a function of incident momentum for the angular distribution in the reaction $K^-p \to \Sigma^0\pi^0$. The data of Berley, et al. (Ref. 13) and Armenteros, et al. (Ref. 14) are shown for comparison.

Fig. 10. Legendre coefficients B_ℓ/A_0 (ℓ = 1, 4) as a function of incident momentum for the Σ^0 polarization in the reaction $K^-p \to \Sigma^0\pi^0$. The data of Berley, et al. (Ref. 13) and Armenteros, et al. (Ref. 14) are shown for comparison.

Fig. 11. Differential cross sections (mb/sr) at 0° and 180° for the reactions $K^-p \to \Lambda\pi^0$ (a,b) and $K^-p \to \Sigma^0\pi^0$ (c,d)

Fig. A1. Diagram defining the angles used in the analysis of the reaction $K^-p \to \Sigma^0\pi^0$, $\Sigma^0 \to \Lambda\gamma$.

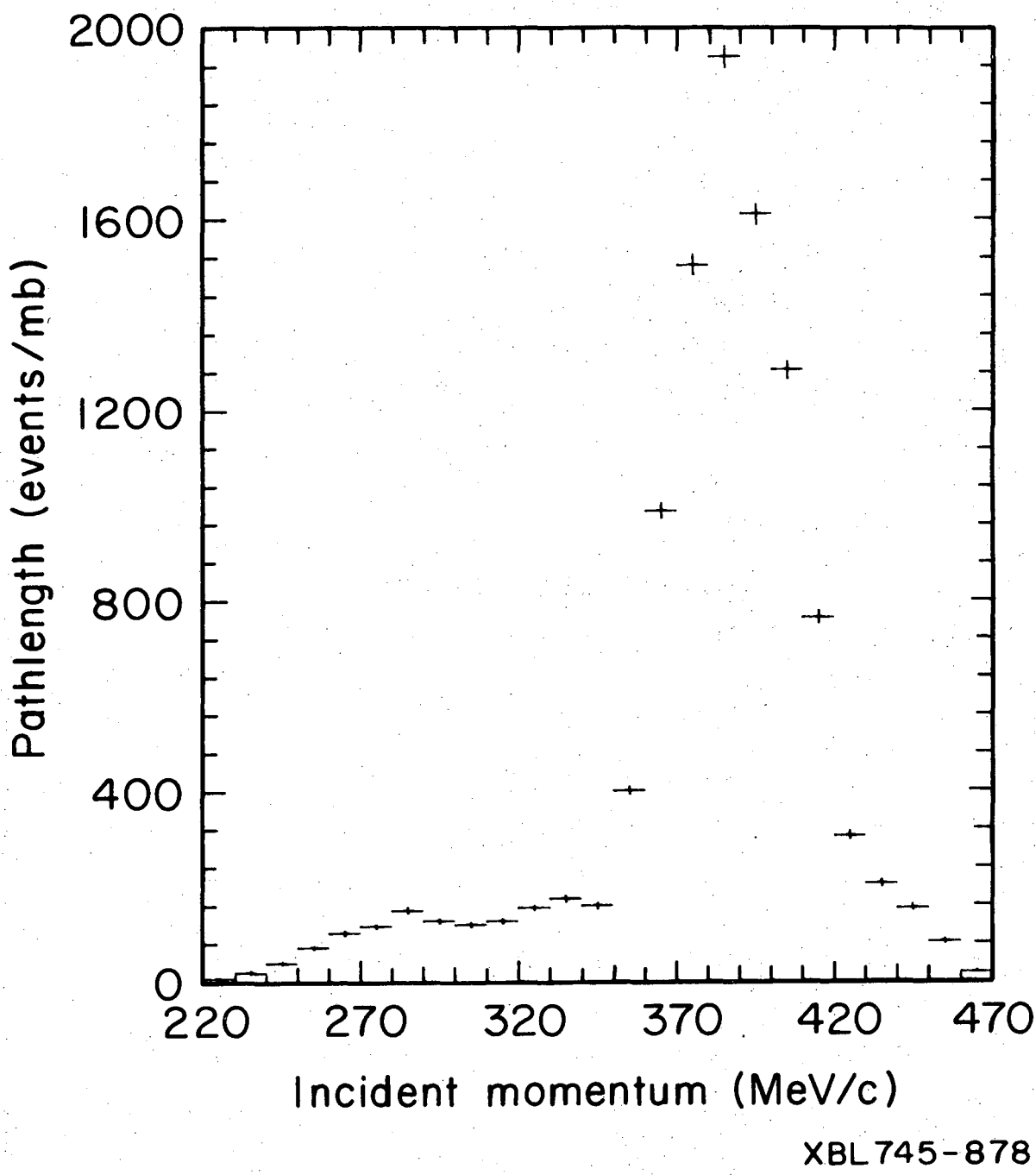
2000
1600
1200
800
400
0
Pathlength (events/mb)
220
270
320
370
420
470
Incident momentum (MeV/c)
XBL745-878

Fig. 1

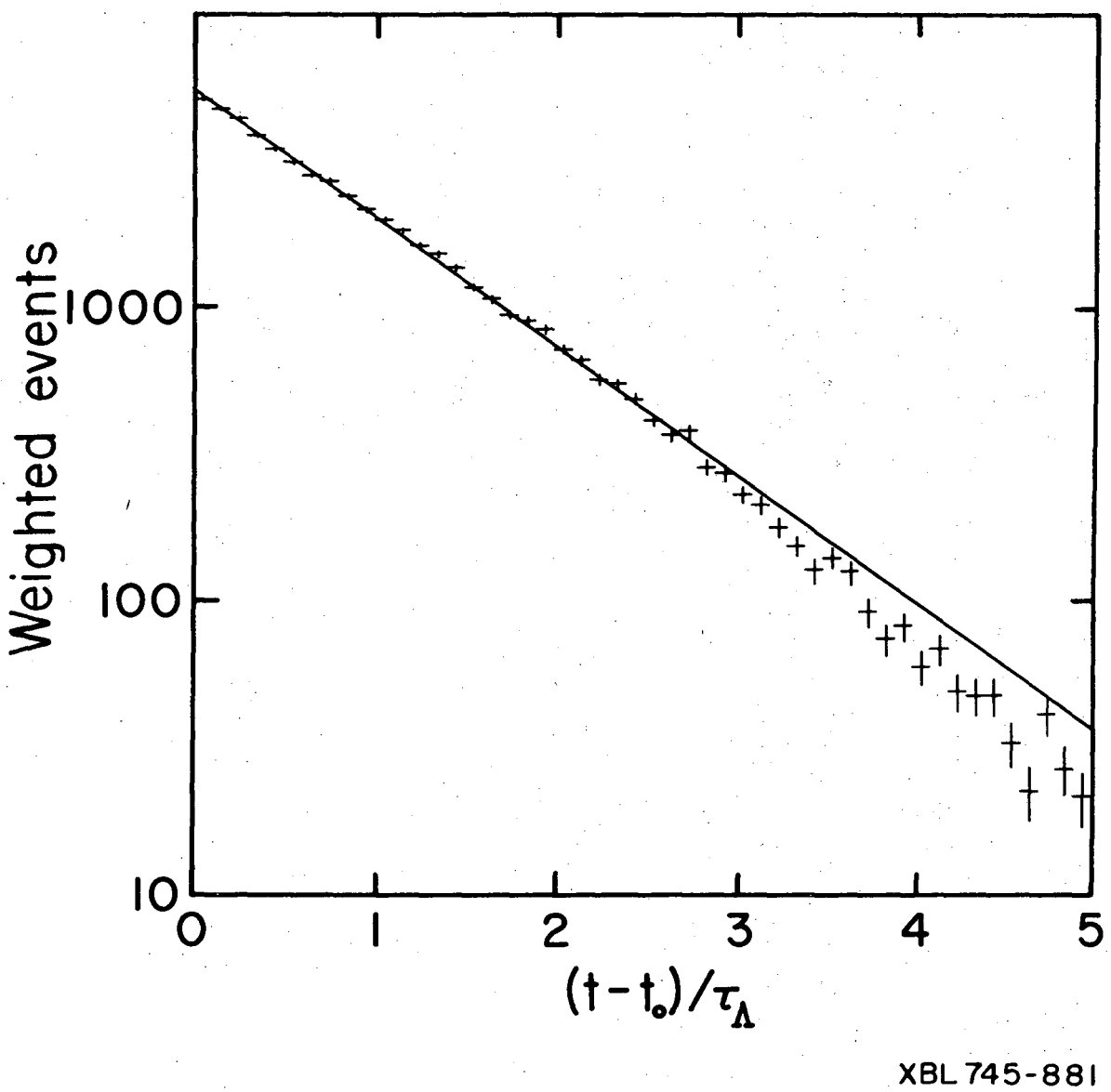
Weighted events
1000
100
10
0
1
2
3
4
5
$(t-t_o)/\tau_\Lambda$
XBL 745-881

Fig. 2

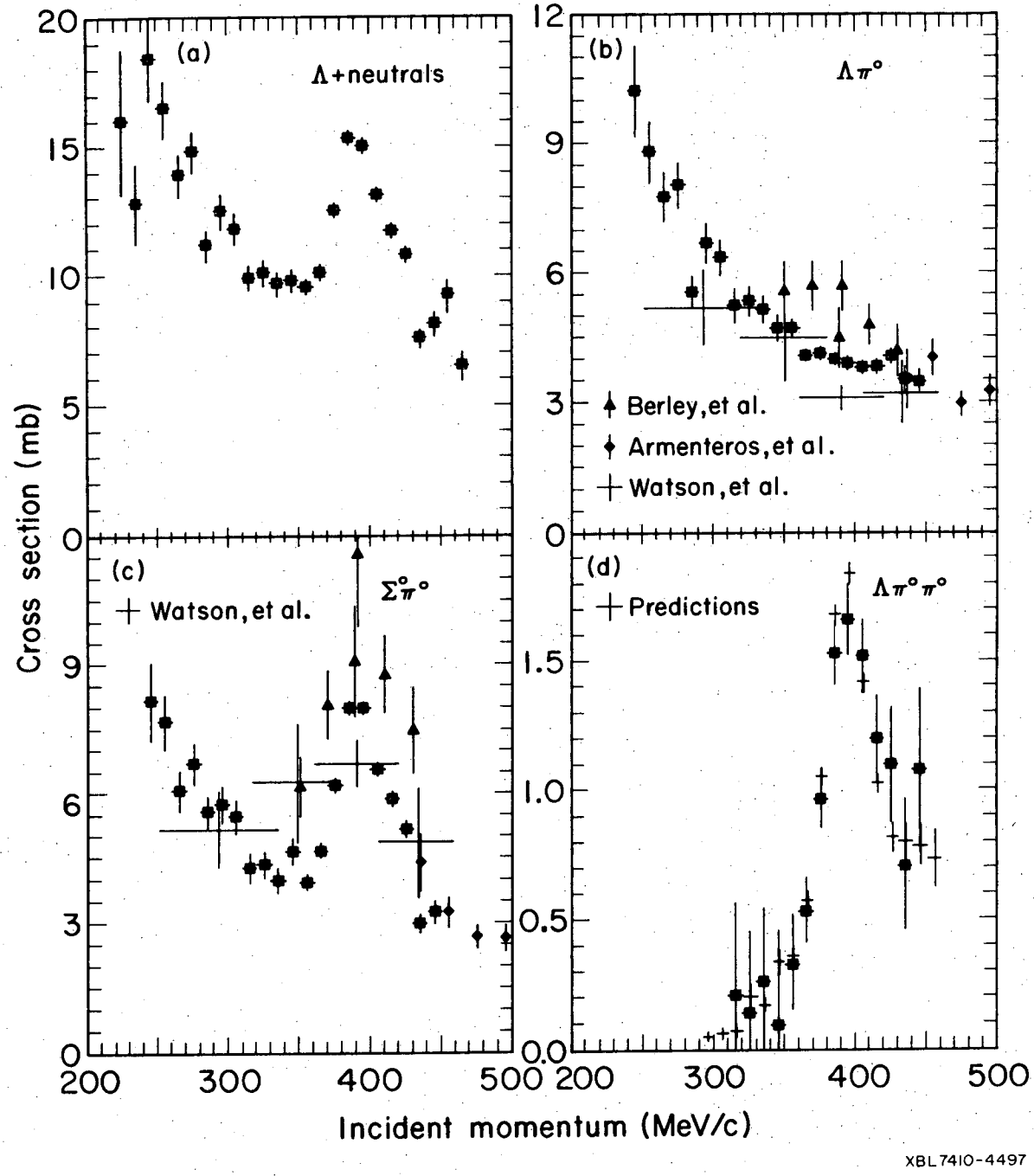
(a)
Λ+neutrals
(b)
Λπ°
Berley,et al.
Armenteros,et al.
Watson,et al.
(c)
Watson,et al.
Σ°π°
(d)
Predictions
Λπ°π°
Cross section (mb)
Incident momentum (MeV/c)
XBL7410-4497

Fig. 3

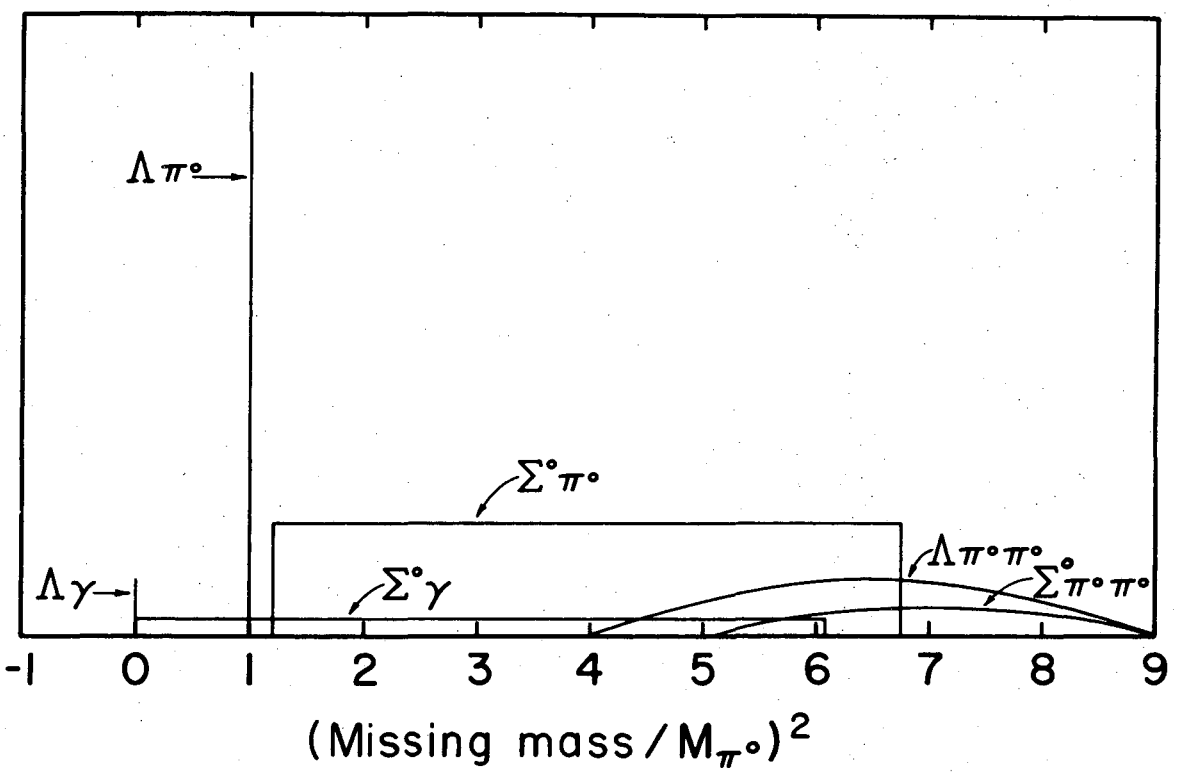

Fig. 4

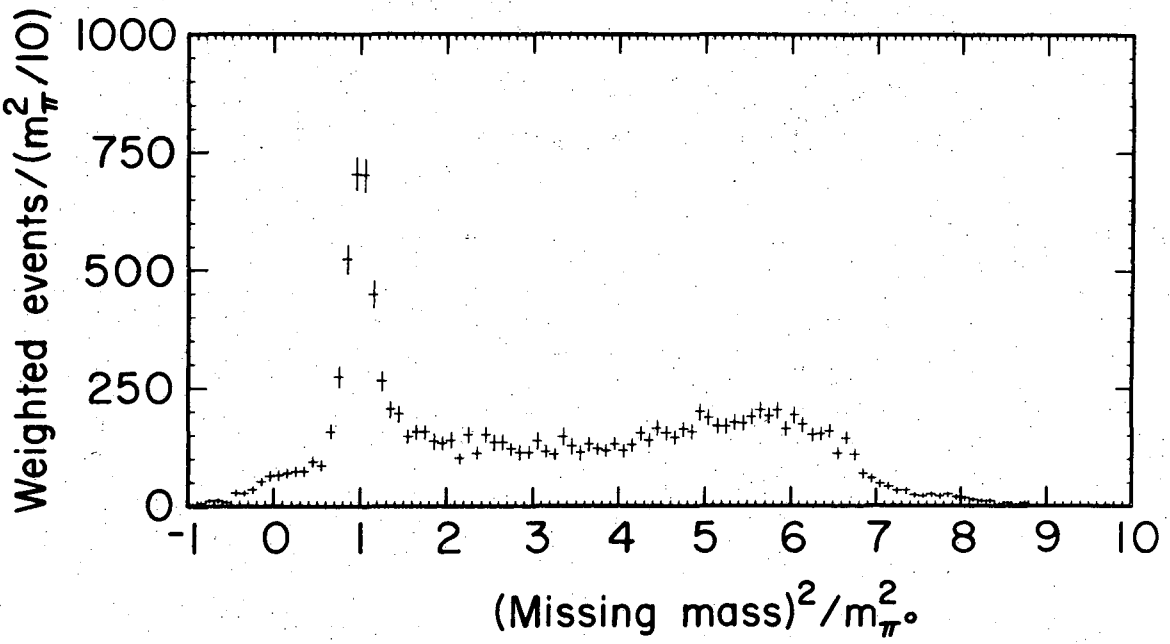
Weighted events/(m_π^2/10)
1000
750
500
250
0
-1
0
1
2
3
4
5
6
7
8
9
10
(Missing mass)^2/m_π^2
XBL745-877

Fig. 5

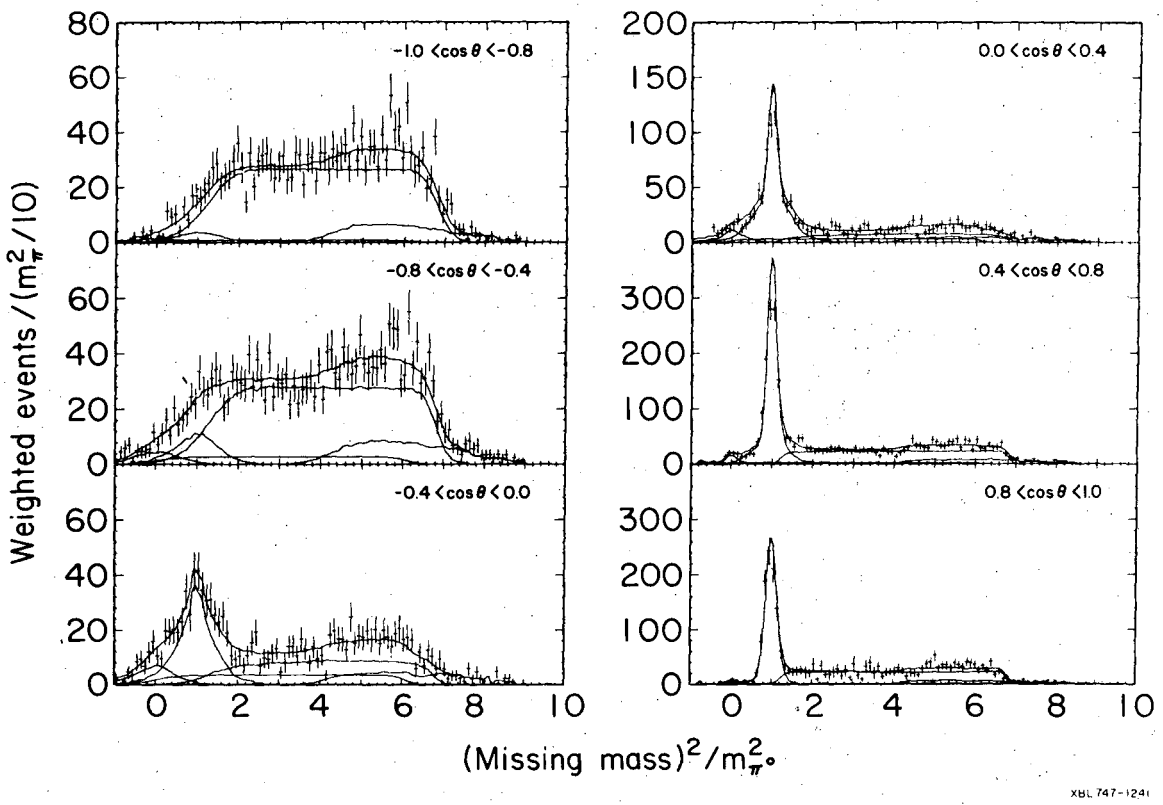
-1.0 <cos θ <-0.8
-0.8 <cos θ <-0.4
-0.4 <cos θ <0.0
0.0 <cos θ <0.4
0.4 <cos θ <0.8
0.8 <cos θ <1.0
Weighted events /(m²π/10)
(Missing mass)²/m²π
XBL 747-1241

Fig. 6

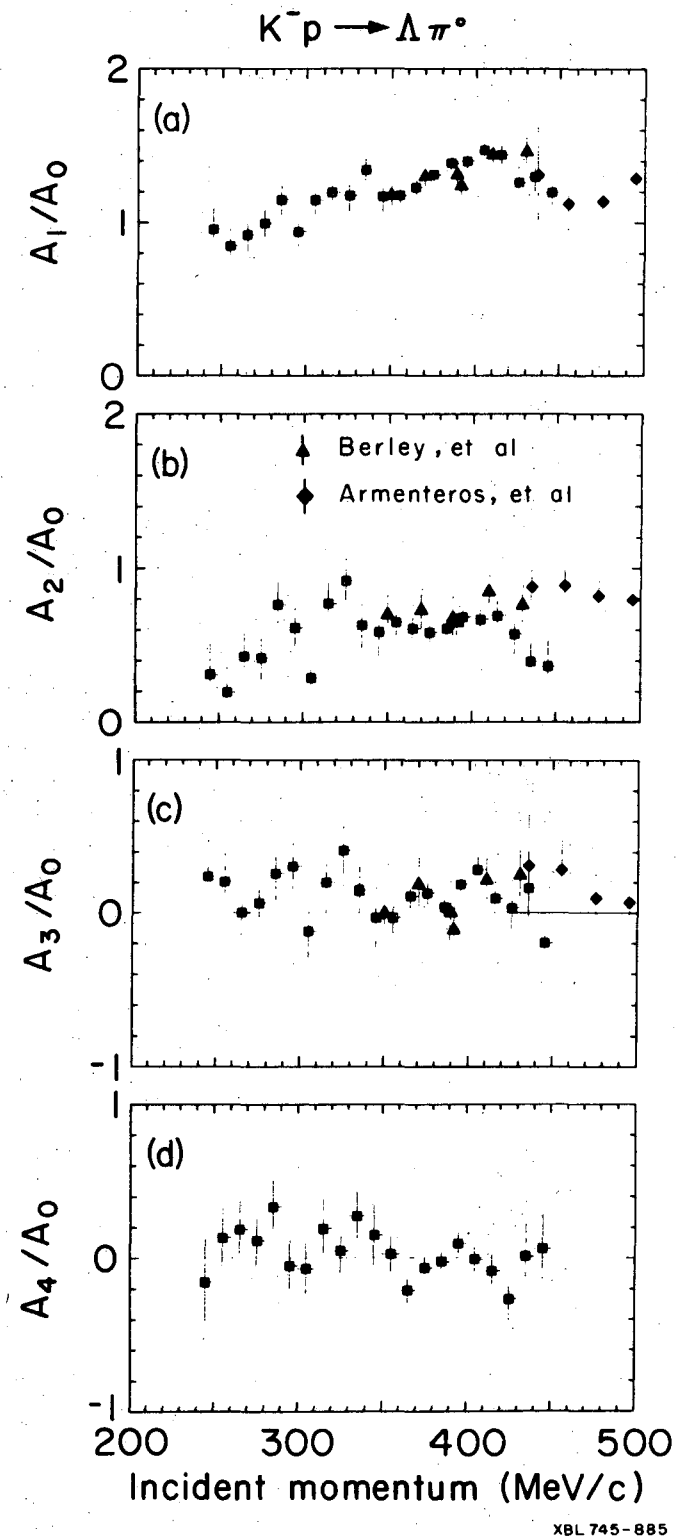
K⁻p → Λπ°
(a)
(b)
(c)
(d)
A1/A0
A2/A0
A3/A0
A4/A0
Berley, et al
Armenteros, et al
2
1
0
-1
200
300
400
500
Incident momentum (MeV/c)
XBL 745-885

Fig. 7

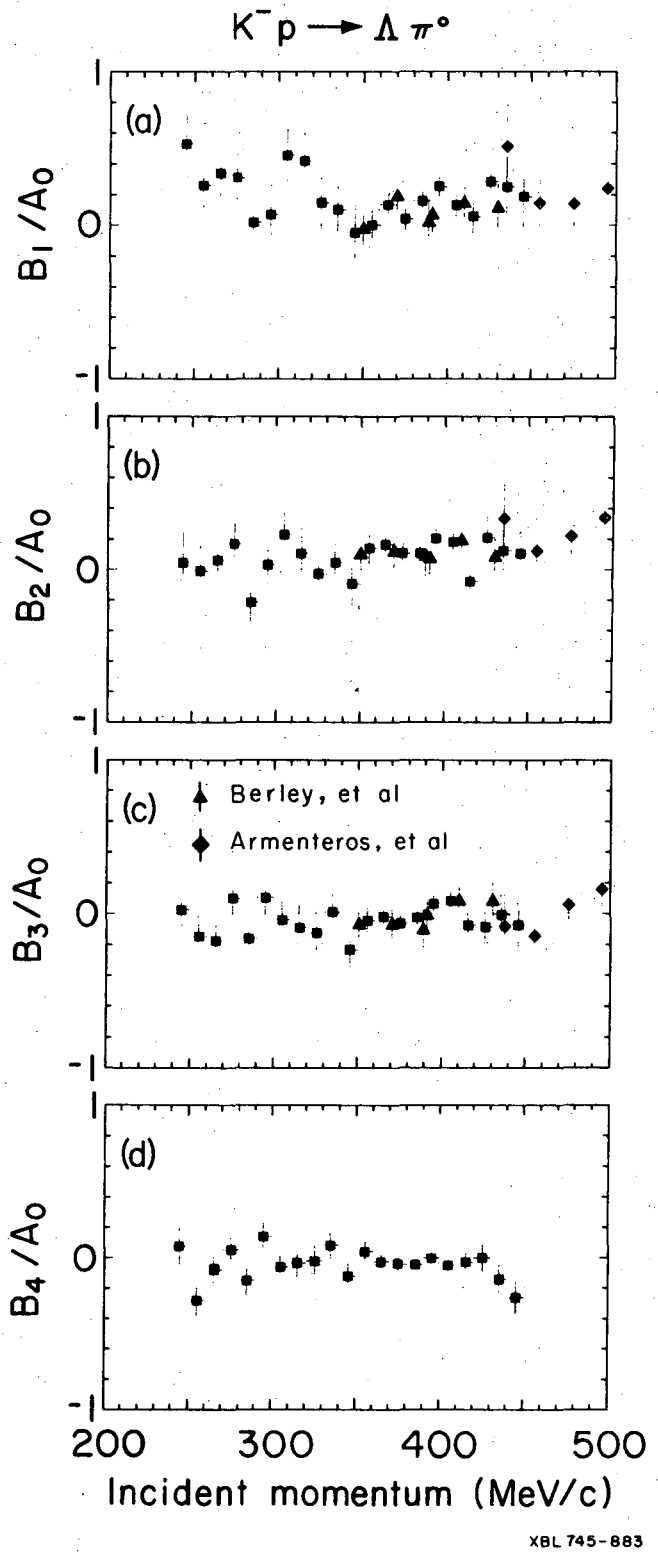
K⁻p → Λ π°
(a)
B1 /A0
(b)
B2 /A0
(c)
Berley, et al
Armenteros, et al
B3/A0
(d)
B4 /A0
0
1
-1
200
300
400
500
Incident momentum (MeV/c)
XBL 745-883

Fig. 8

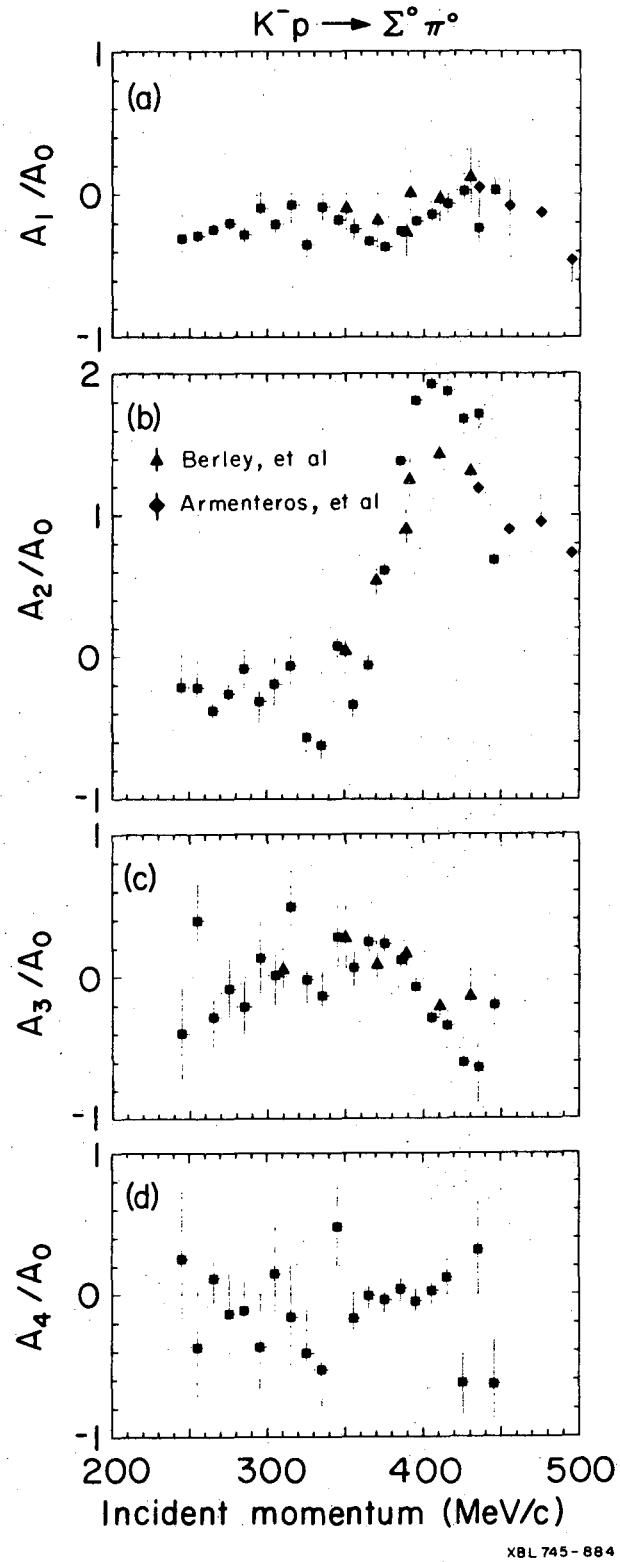
K⁻p → Σ°π°
(a)
A1 /A0
(b)
Berley, et al
Armenteros, et al
A2/A0
(c)
A3 /A0
(d)
A4 /A0
1
0
-1
2
200
300
400
500
Incident momentum (MeV/c)
XBL 745-884

Fig. 9

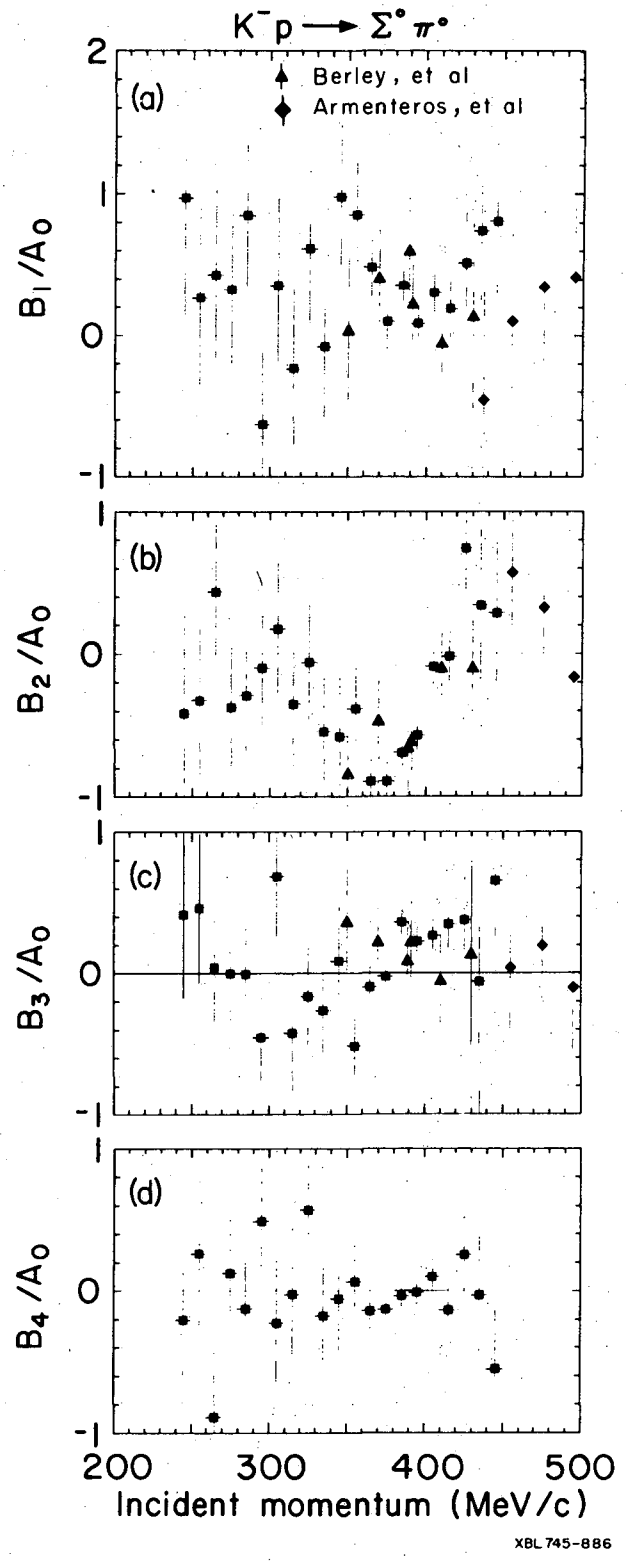
$K^- p \longrightarrow \Sigma^\circ \pi^\circ$
Berley, et al
Armenteros, et al
(a)
(b)
(c)
(d)
B_1/A_0
B_2/A_0
B_3/A_0
B_4/A_0
2
1
0
-1
200
300
400
500
Incident momentum (MeV/c)
XBL 745-886

Fig. 10

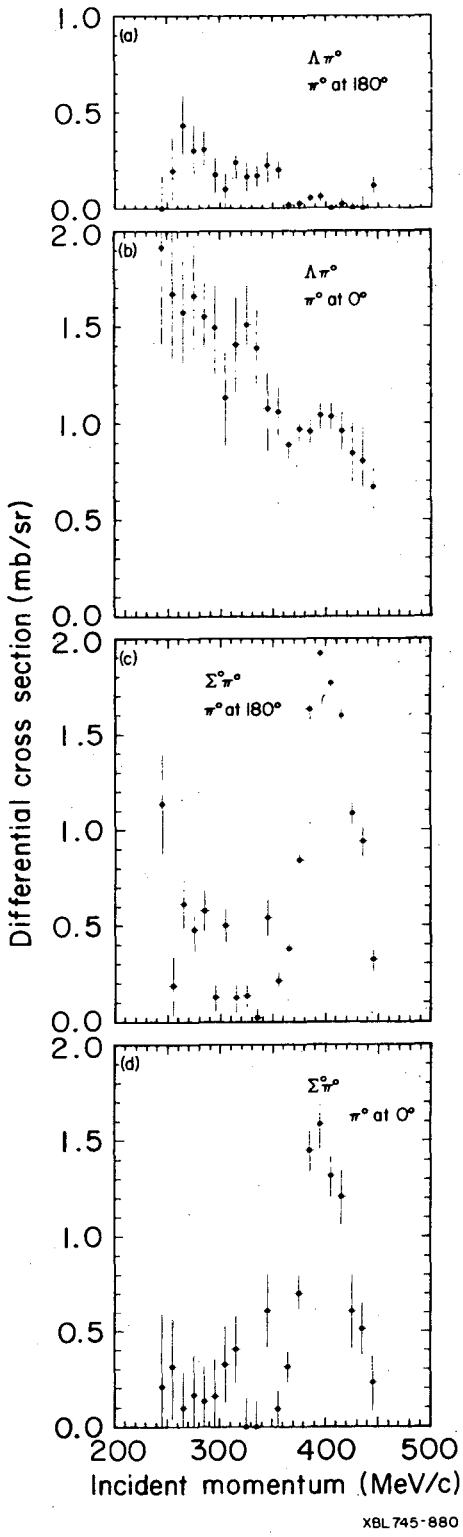
(a)
Λπ°
π° at 180°
(b)
Λπ°
π° at 0°
(c)
Σ°π°
π° at 180°
(d)
Σ°π°
π° at 0°
Differential cross section (mb/sr)
Incident momentum (MeV/c)
XBL745-880

Fig. 11

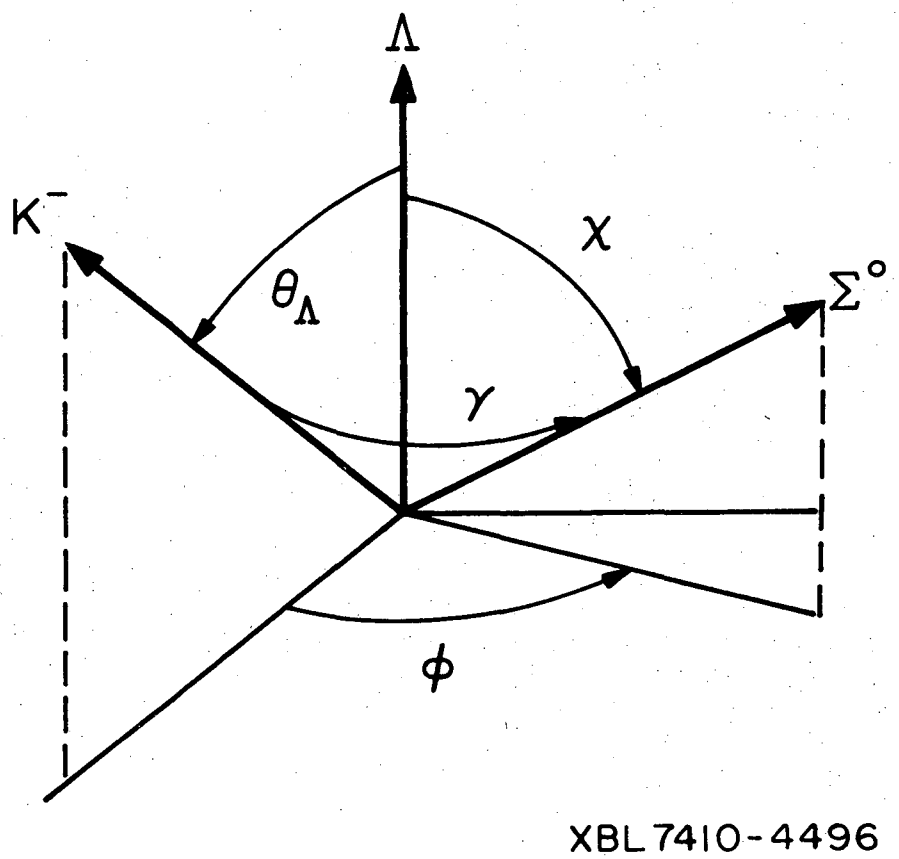

Fig. 12

TECHNICAL INFORMATION DIVISION
LAWRENCE BERKELEY LABORATORY
UNIVERSITY OF CALIFORNIA
BERKELEY, CALIFORNIA 94720